Treg-Dominant Tumor Microenvironment Is Responsible for Hyperprogressive Disease after PD-1 Blockade Therapy

Hiroaki Wakiyama, Takuya Kato, Aki Furusawa, Ryuhei Okada, Fuyuki Inagaki, Hideyuki Furumoto, Hiroshi Fukushima, Shuhei Okuyama, Peter L. Choyke, and Hisataka Kobayashi

ABSTRACT

Programmed cell death 1 (PD-1) blockade therapy can result in dramatic responses in some patients with cancer. However, about 15% of patients receiving PD-1 blockade therapy experience rapid tumor progression, a phenomenon termed "hyperprogressive disease" (HPD). The mechanism(s) underlying HPD has been difficult to uncover because HPD is challenging to reproduce in animal models. Near-infrared photoimmunotherapy (NIR-PIT) is a method by which specific cells in the tumor microenvironment (TME) can be selectively depleted without disturbing other cells in the TME. In this study, we partially depleted $CD8^+$ T cells with NIR-PIT by targeting the CD8β antigen thereby temporarily changing the balance of T-cell subsets in two different syngeneic tumor models. PD-1 blockade in these models led to rapid tumor progression compared with controls. $CD3\varepsilon^+CD8\alpha^+/CD3\varepsilon^+CD4^+FoxP3^+$ (T_{eff}/T_{reg}) ratios in the PD-1 and NIR-PIT groups were lower than in controls. Moreover, in a bilateral tumor model, low-dose CD8β-targeted NIR-PIT with anti–PD-1 blockade showed rapid tumor progression only in the tumor exposed to NIR light. In this experiment CD8β-targeted NIR-PIT in the exposed tumor reduced local $CD8^+$ T cells resulting in a regulatory T-cell (Treg)–dominant TME. In conclusion, this reports an animal model to simulate the Treg-dominant TME, and the data generated using the model suggest that HPD after PD-1 blockade therapy can be attributed, at least in part, to imbalances between effector T cells and Tregs in the TME.

Introduction

Immune checkpoint inhibitors (ICI) have become a major component of cancer therapy. However, ICIs are not effective in all patients and responses are difficult to predict. The objective response rate (11.2%–31.7%) in solid tumors is frustratingly low (1). Moreover, several retrospective studies have recently identified a subset of patients who not only do not benefit from ICI, but rather, demonstrate rapid progression of their disease, a phenomenon termed "hyperprogressive disease" (HPD; refs. 1–4). HPD has been difficult to study because animal models have been lacking.

Kamada and colleagues (5) have reported that programmed cell death 1 (PD-1) blockade or deficiency enhances the proliferation and immunosuppressive activity of $PD\text{-}1^+$ effector regulatory T cells (Treg). This paradoxical upregulation of immunosuppressive mechanisms could be caused by an imbalance of T-cell subtypes in the tumor microenvironment (TME), whereby cytotoxic T cells are relatively scarce compared with the more abundant immunosuppressive Tregs. We hypothesized that such an imbalance could play a critical role in HPD.

Molecular Imaging Branch, Center for Cancer Research, National Cancer Institute, NIH, Bethesda, Maryland.

Corresponding Author: Hisataka Kobayashi, Molecular Imaging Branch, Center for Cancer Research, National Cancer Institute, NIH, 10 Center Drive, Bethesda, MD 20892. Phone: 240-858-3069; Fax: 240-541-4527; E-mail: kobayash@mail.nih.gov

Cancer Immunol Res 2022;10:1386–97

doi: 10.1158/2326-6066.CIR-22-0041

Near-infrared photoimmunotherapy (NIR-PIT) is a newly developed cancer treatment (6, 7) that uses an antibody–photoabsorber conjugate (APC). It can also be used to deplete selected cells in the TME. Once injected, the APC binds to target cells and subsequent NIR light exposure activates the dye, IRDye700DX (IR700). NIR-PIT causes rapid and selective killing of target cells (8, 9). Although NIR-PIT has been mainly directed against tumor antigens on cancer cells, it can also be directed against any cell in the TME (10). $CD8^+$ effector T cells constitutively express CD8α and CD8β. Given that some subsets of dendritic cells (DC) express CD8α, typically as αα-homodimers, whereas αβ-heterodimers are typical of T cells (11), CD8β-targeted NIR-PIT would selectively deplete $CD8^+$ T cells without affecting DCs or other lymphocytes, including $CD4^+$ T cells such as Tregs. The degree of cell depletion can be regulated by light exposure. CD8β-targeted NIR-PIT is expected to alter the balance between $CD8^+$ T cells and Tregs in the TME. In this study, we aimed to investigate whether CD8β-targeted NIR-PIT could induce a Treg-dominant TME that could paradoxically result in HPD after PD-1 therapy, thus creating a model by which HPD can be better studied.

Materials and Methods

Reagents

The water-soluble, silica-phthalocyanine derivative IRDye700DX (IR700) NHS ester was obtained from LI-COR Biosciences (cat. #929–70010; Lincoln). A mouse CD8β–specific monoclonal antibody (mAb) (clone 53–5.8) and a mouse PD-1 (CD279)–specific mAb (clone RMP1–14) were purchased from Bio X Cell. All other chemicals were of reagent grade.

Synthesis of IR700-conjugated anti-CD8β

Conjugation of IR700 with mAb was performed according to a previous report (12). In brief, anti-CD8β (1.0 mg, 6.7 nmol/L) was incubated with IR700 NHS ester (65.1 μg, 33.3 nmol, 10 mmol/L in DMSO) in 0.1 mol/L Na_2HPO_4 (pH 8.5) at room temperature for 1 hour. The mixture was purified with a PD-10 column with Sephadex G25 resin (cat. #17085101, Cytiva). The protein concentration was determined with a Coomassie Plus Protein Assay Kit (cat. #PI23236, Thermo Fisher Scientific) by measuring the absorption at 595 nm with UV-Vis (8453 Value System; Agilent Technologies). Herein, we abbreviate IR700 conjugated to anti-CD8β as anti–CD8β-IR700. The success of conjugation was verified by SDS-PAGE with a 4%−20% gradient polyacrylamide gel (Life Technologies). Nonconjugated antibody and ultrapure water were used for positive and negative controls, respectively. After electrophoresis at 80 V for 2 hours, the gel was imaged with a Pearl Imager (LI-COR Biosciences) using the 700 nm fluorescence channel. The gel was then stained with Colloidal Blue Stain kit (cat. #LC6025, Thermo Fisher Scientific) to compare the molecular weight of the conjugate with that of nonconjugated antibody. Stained gels were imaged with ChemiDoc Gel Imaging System (Bio-Rad), the molecular weights of antibodies were determined on the basis of the relative position to 10–250 kDa Pre-Stained Protein Marker (cat. #65–0681, Crystalgen).

CD8$^+$ T cell–specific binding analysis

Lymph nodes isolated from non–tumor-bearing C57BL/6 mice (strain #000664, The Jackson Laboratory) were gently mashed on a petri dish and passed through a 70-μm cell strainer. Single-cell suspensions were seeded into 12-well plates (7.0×10^5 cells per well) and incubated with RPMI-1640 (cat. #11875–093, Thermo Fisher Scientific) containing 10 μg/mL of anti-CD8β–IR700 for 1 hour at 37°C. Then, the CD8α$^-$/CD3ε$^+$ and CD8α$^+$/CD3ε$^+$ populations were analyzed by flow cytometry (see Flow cytometry analysis). To confirm the specific binding of anti–CD8β-IR700, a blocking study was performed whereby 10 times the amount of nonconjugated anti-CD8β was added to samples 1 hour before the incubation with the APC.

Fluorescence microscopy

To detect the antigen-specific localization and effect of CD8β-targeted NIR-PIT, fluorescence microscopy was performed. T cells were isolated from spleen resected from a female C57BL/6 mouse (strain #000664) using EasySep Mouse T-Cell Isolation Kit (cat. #19851, StemCell Technologies Inc.) according to the manufacturer's protocol. KIRAVIA Blue 520-conjugated anti–mouse CD4 (cat. #100478, BioLegend) at 5 μg/mL and anti-CD8β–IR700 at 10 μg/mL were added to the cell suspension with staining buffer (PBS containing no calcium or magnesium with 1% FBS) and incubated for 1 hour at 4°C. After washing, cells were resuspended with staining buffer containing 10 μg/mL propidium iodide (PI; cat. #P4864, Millipore Sigma). Then, cells were seeded on a glass slide overlaid with a cover glass. NIR laser-light (690 nm, 100 mW/cm^2) was applied at 30 J/cm^2 using an ML7710 laser system (Modulight) and serial microscopy was obtained using an IX81 microscope (Olympus) and cellSense Dimension software (version 1.15, Olympus). The filter set to detect IR700 consisted of a 590 to 650 nm excitation filter, a 665 to 740 nm band pass emission filter. The filter set to detect KIRAVIA Blue 520 consisted of a 460 to 490 nm excitation filter, a 510 to 550 nm band pass emission filter. The filter set to detect PI consisted of a 532.5 to 587.5 nm excitation filter, a 607.5 to 682.5 nm band pass emission filter. Transmitted light differential interference contrast images (DIC) were also acquired.

Ex vivo NIR-PIT for lymph node cells

Lymph node cells isolated from non–tumor-bearing mice, as described in CD8$^+$ T cell–specific binding analysis, were seeded into 12-well plates (7.0×10^5 cells per well) and incubated with RPMI-1640 containing 10 μg/mL of anti–CD8β-IR700 for 2 hours at 37°C. After washing with PBS, phenol-red-free RPMI medium (cat. #11853–030, Thermo Fisher Scientific) was added. NIR light (690 nm, 100 mW/cm^2) was applied at 0, 1, 5, 10, 20, and 30 J/cm^2 using an ML7710 laser system (Modulight). One hour after NIR-PIT, the CD8α$^+$/CD3ε$^+$ ratio in the remaining cells was analyzed by flow cytometry (see Flow cytometry analysis).

Cell culture

The MC38 cell line (murine colon cancer) was generously provided by Dr. Thomas Waldmann, NIH in 2005. The MOC2 cell line (murine oral carcinoma) was purchased from Kerafast in 2020. MC38 cells stably expressing luciferase (MC38-luc) and MOC2 cells stably expressing luciferase (MOC2-luc) were generated via stable transduction with RediFect Red-Fluc lentivirus (CLS960002, PerkinElmer) per the manufacturer's recommendations. MC38 and MC38-luc were cultured in RPMI-1640 medium supplemented with 10% FBS (cat. #16000–044, Thermo Fisher Scientific), 100 IU/mL penicillin and 100 μg/mL streptomycin (cat. #15140122, Thermo Fisher Scientific). MOC2-luc cells were cultured in media as previously described (13). MOC2 and MOC2-luc were cultured in 2:1 mixture of IMDM and Ham's Nutrient Mixture F12 (cat. #16777–184 and cat. #16777–141, Cytiva) with 5% FBS, 100 IU/mL penicillin and 100 μg/mL streptomycin, 5 ng/mL EGF (cat. #01–107, Millipore Sigma), 400 ng/mL hydrocortisone (cat. #H0135–1MG, Millipore Sigma), and 5 ng/mL insulin (cat. #I0516–5ML, Millipore Sigma). All cell lines were authenticated by STR profiling and tested for *Mycoplasma* via CellCheck 19 plus service (IDEXX BioAnalytics) in 2021. Cells were frozen down soon after the authentication and *Mycoplasma* testing, and thawed to be used in this study. After thawing, cells were maintained in culture for no more than 30 passages.

Animal and tumor models

All *in vivo* procedures were approved by the National Cancer Institute (NCI) Animal Care and Use Committee. Six- to 8-week-old female wild-type C57BL/6 mice (strain #000664) were purchased from The Jackson Laboratory. Tumors were established via subcutaneous injection of 5×10^5 cells for MC38 and 1×10^6 cells for MOC2-luc in the caudal flank. For NIR-PIT treatments and bioluminescence imaging (BLI), mice were anesthetized with inhaled 2% to 3% isoflurane and/or via i.p. injection of 0.75 mg of sodium pentobarbital (Nembutal Sodium Solution, Ovation Pharmaceuticals Inc.). The hair overlying the tumor site was removed before NIR light irradiation and imaging studies (see *in vivo* PD-1 blockade with CD8β-targeted NIR-PIT). For determination of tumor volume, the greatest longitudinal diameter (length), and the greatest transverse diameter (width) were measured with a caliper. Tumor volume was calculated using the modified ellipsoid formula as follows: tumor volume = length $\times$ width^2 $\times$ 0.5. Tumor size was measured three times a week until the tumor volume reached 2,000 mm^3 or the length reached 2 cm, whereupon the mice were euthanized with inhalation of carbon dioxide gas.

Systemic effects of anti–CD8β-IR700

To examine the systemic effects of anti-CD8β–IR700, non–tumor-bearing C57BL/6 mice (strain #000664) were randomized into 2 groups as follows: (i) no treatment (Control); (ii) 5 μg anti-CD8β–IR700 administered intravenously (APC i.v.). 20 μL whole-blood samples were collected from the facial veins of mice anesthetized as described previously in animal and tumor models ($n = 10$) immediately before, and after (1 day, 1week, 2 weeks, and biweekly thereafter) anti–CD8β-IR700 administration. Red blood cells were removed by incubating with RBC lysis buffer (cat. #420301, BioLegend). Then, the CD8α^+/CD45$^+$CD3ε^+ ratio was analyzed by flow cytometry (see Flow cytometry analysis).

Ex vivo NIR-PIT with MC38 tumor

Single-cell suspensions from MC38 tumor samples were prepared using the following protocol. Whole tumors were minced and incubated in RPMI medium containing collagenase type IV (cat. #LS004188, 1 mg/mL; Worthington Biochemical) and DNaseI (cat. #11284932001, 20 μg/mL; Millipore Sigma) at 37°C for 60 minutes. Tumors were then gently dissociated and filtered with a 70 μm cell strainer (Corning). 1.0×10^6 cells were incubated with RPMI-1640 containing 10 μg/mL of anti–CD8β-IR700 for 2 hours at 37°C. After washing with PBS, phenol-red–free medium was added. NIR light (690 nm, 100 mW/cm^2) was applied at 10 J/cm^2 using an ML7710 laser system and the cells were then incubated for 60 minutes at 37°C. The cells were then analyzed by flow cytometry (see Flow cytometry analysis).

Analysis of tumor-infiltrating CD8$^+$ T cells after CD8β-targeted NIR-PIT

To evaluate the efficacy of CD8β-targeted NIR-PIT for tumor-infiltrating CD8$^+$ T cells, tumor-bearing mice were randomized into 3 groups as follows: (i) no treatment (Control); (ii) anti–CD8β-IR700 i.v. injection and no NIR light exposure (i.v. only); (iii) anti–CD8β-IR700 i.v. injection and NIR light exposure (NIR-PIT). 5-μg anti-CD8β–IR700 was injected 8 days after tumor inoculation and NIR light (690 nm, 100 mW/cm^2, 10 J/cm^2) was administered on day 9 after tumor inoculation for MC38 tumors. 30-μg anti–CD8β-IR700 was injected 7 days after tumor inoculation and NIR light (690 nm, 100 mW/cm^2, 30 J/cm^2) was administered on day 8 after tumor inoculation for MOC2-luc tumors. Tumors, left axillary lymph nodes, and spleens were harvested 1 hour after NIR light exposure for flow cytometry. Single-cell suspensions from tumor samples and lymph nodes were prepared using the protocols described above. Spleen was gently mashed on the petri dish, incubated in RBC lysis buffer (cat. #00–4300–54, Thermo Fisher Scientific) to remove red blood cells, and then passed through a 70-μm cell strainer. The CD8α^+/CD45$^+$CD3ε^+ ratio (T_{eff}) and CD8α^+/CD45$^+$CD3$^-$ ratio (DC) for each tumor was determined by flow cytometry. The CD8α^+/CD3ε^+PD-1$^+$ ratio and CD4$^+$FoxP3$^-$/CD3ε^+PD-1$^+$ ratio and CD4$^+$FoxP3$^+$/CD3ε^+PD-1$^+$ of MC38 tumors after CD8-targeted NIR-PIT were determined by flow cytometry analysis. The treatment regimens are also shown as diagrams together with each experimental result.

In vivo PD-1 blockade with CD8β-targeted NIR-PIT

To evaluate the effect of anti–PD-1 therapy after the elimination of CD8$^+$ T cells in the TME, tumors were implanted unilaterally and mice were randomized into 4 groups: (i) no treatment (Control); (ii) i.p. injection of anti–PD-1 (PD-1; clone RMP1–14, Bio X Cell, 200 μg/injection as indicated in figures); (iii) anti–CD8β-IR700 i.v. injection and NIR light exposure (CD8-PIT); (iv) anti–CD8β-IR700 i.v. injection and NIR light exposure, and i.p. injection of anti–PD-1 (Combination). In mice bearing bilateral MC38 tumors, only right-sided tumors were irradiated with NIR light, left-sided tumors were shielded with aluminum foil and thus, did not receive NIR light. 5-μg anti–CD8β-IR700 was injected 8 days after tumor inoculation and NIR light (690 nm, 100 mW/cm^2, 10 J/cm^2) was administered on day 9 after tumor inoculation for MC38 tumors. 30 μg anti-CD8β–IR700 was injected 7 days after tumor inoculation and NIR light (690 nm, 100 mW/cm^2, 30 J/cm^2) was administered on day 8 after tumor inoculation for MC38-luc tumors. 30 μg anti–CD8β-IR700 was injected 7 days after tumor inoculation, and NIR light (690 nm, 100 mW/cm^2, 30 J/cm^2) was administered on day 8 after tumor inoculation for MOC2-luc tumors. Anti–PD-1 was administered via i.p. injection on days 9 and 12 for MC38 tumors and on day 8 and 11 for MOC2-luc tumors. Dorsal fluorescence images of IR700 were obtained with the 700 nm fluorescence channel of the Pearl Imager (LI-COR Biosciences). The images were taken before and after NIR-PIT. Pearl Cam Software (LI-COR Biosciences) was used for analyzing fluorescence. Regions of interest (ROI) were placed on the tumor. Acute effects of the treatments were evaluated with BLI for MOC2-luc tumors. For BLI, 200 μL of 15 mg/mL D-luciferin (LUCK-1g, Gold Biotechnology) was injected intraperitoneally, and mice were analyzed with a BLI system (Photon Imager; Biospace Lab) and M3 Vision Software (Biospace Lab) for luciferase activity (14). ROIs were set on the entire tumor. MC38 tumors of each group were harvested on day 13 to analyze CD8$^+$ T cells and Tregs with flow cytometry in unilateral and bilateral tumor models. In addition, tumors and draining lymph nodes from each group were collected on day 13 and flow cytometry analysis of DC activation/maturation was performed in the MC38 unilateral tumor model. MOC2-luc tumors were harvested on day 13, and the distribution of CD8$^+$ T cells and Tregs was analyzed by multiplex immunohistochemistry (IHC).

Flow cytometry analysis

Single-cell suspensions from tumor samples, lymph nodes, and spleen were prepared using the protocols described above. 3.0×10^6 cells were stained and data for 3.0×10^5 cells were collected for each tumor. 5.0×10^5 cells were stained and data for 1.0×10^5 cells were collected for each lymph node and spleen. The cells were stained with the following antibodies: anti-CD3ε (clone 145–2C11), anti–I-A/I-E (M5/114.15.2), anti-CD11c (N418), anti-CD86 (GL-1), and anti–PD-1 (29F.1A12) obtained from Biolegend; and anti-CD45 (clone 30-F11), anti-CD8α (clone 53–6.7), anti-FoxP3 (clone FJK-16s), anti-CD4 (clone RM4–5), anti-CD11c (N418), anti-F4/80 (BM8), anti-CD40 (1C10), anti-CD80 (16–10A1), and Ki67 (SolA15) were obtained from eBioscience. Staining for FoxP3 and Ki67 was performed after fixation and permeabilization using the FoxP3 Transcription Factor Staining Buffer Set (cat. #00–5523–00, Thermo Fisher Scientific). Dead cells were removed from analysis based on fsc, ssc, and staining with Fixable Viability Dye eFluor 506 or 780 (cat. #65–0866–14 or #65–0865–14, Thermo Fisher Scientific). Cell types were determined as following; CD8$^+$ T cells: CD45$^+$CD3ε^+CD8α^+, Tconv: CD45$^+$CD3ε^+CD4$^+$FoxP3$^-$, Treg: CD45$^+$CD3ε^+CD4$^+$FoxP3$^+$, DC: CD45$^+$F4/80$^-$CD11c$^+$I-A/I-E$^+$. The stained cells were evaluated using a FACSLyric (BD Biosciences) and the data were analyzed with FlowJo software (version 10.8.1, FlowJo LLC).

Multiplex IHC

Multiplex IHC to analyze the distribution of CD8$^+$ T cells and Tregs in MOC2-luc tumors harvested after PD-1 blockade together with CD8β-targeted NIR-PIT was performed in FFPE sections as previously described (15) using Opal Automation IHC Kit (cat. #NEL821001KT, Akoya Biosciences) and Bond RXm auto stainer (Leica Biosystems). The following antibodies were used: anti-CD8 (clone EPR20305;

Abcam), anti-CD4 (clone EPR19514; Abcam), anti-FoxP3 (clone 1054 C; Novus Biologicals) and anti–pan-cytokeratin (CK; rabbit poly; Bioss). Stained slides were mounted with ProLong Diamond Antifade Mountant (cat. #P36970, Thermo Fisher Scientific) and imaged with Mantra Quantitative Pathology Workstation (Akoya Biosciences). The images were analyzed with inForm Tissue Finder software (ver. 2.5.1, Akoya Biosciences). To segment tissue, trainable tissue segmentation feature was used. CK was used to mark tumor tissue. On the basis of the expression of CK, the tissue area was split into "Stroma" and "Tumor" for T-cell counting. Adoptive

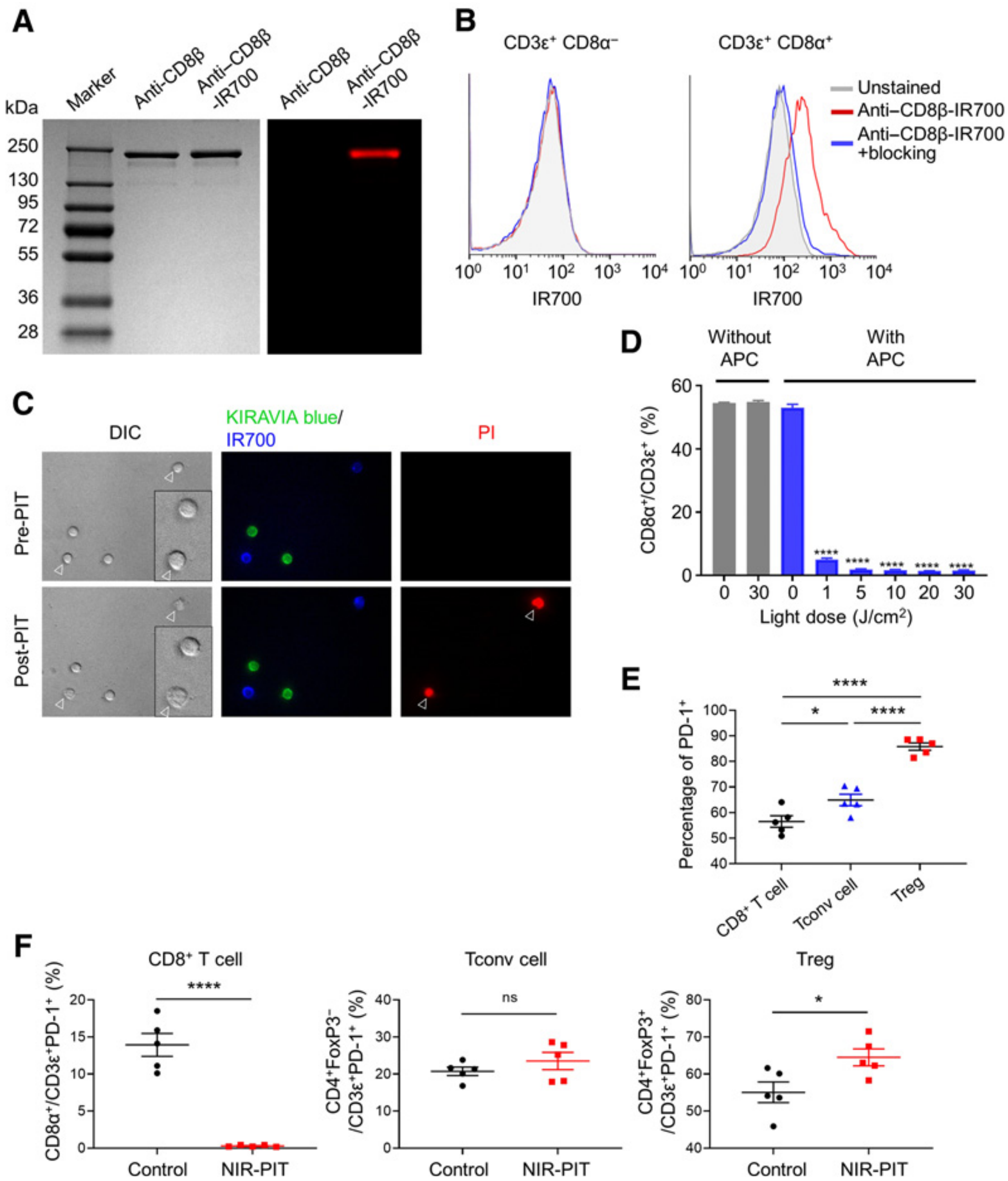

Figure 1.

Conjugation of IR700 to anti-CD8β and evaluation of *ex vivo* NIR-PIT. **A,** Evaluation of anti-CD8β–IR700 by SDS-PAGE (left, Colloidal Blue staining; right, 700-nm fluorescence). The same amount of nonlabeled anti-CD8β was used as a control. **B,** The binding of anti–CD8β-IR700 to lymph node cells was analyzed by flow cytometry. CD3ε$^+$CD8α$^+$ cells showed enhanced IR700 fluorescence signal after incubation with anti–CD8β-IR700. CD8β-blocking antibody was added to some wells to validate CD8β-specific staining. **C,** Fluorescence microscopy was performed before and after CD8β-targeted NIR-PIT using T cells isolated from normal lymph nodes. Anti–CD8β-IR700, anti-CD4 KIRAVIA blue, and PI are shown in blue, green, and red, respectively. After NIR-light irradiation, anti–CD8β-IR700 bound T cells showed swelling, and stained positive for PI (indicated by open arrowhead). A representative example from three independent experiments is shown. **D,** *Ex vivo* NIR-PIT. T cells from the lymph node were incubated with anti–CD8β-IR700 and irradiated with NIR light in various doses ($n = 4$ per group; ****, $P < 0.0001$; vs. untreated control; one-way ANOVA followed by the Dunnett's test). Each value represents means ± SEM. **E,** Lymphocytes in MC38 tumors were analyzed by flow cytometry. PD-1 positivity in CD8$^+$ T cells, CD4$^+$ Tconv, and Tregs is depicted ($n = 5$ per group; *, $P < 0.05$; ****, $P < 0.0001$; one-way ANOVA followed by the Tukey's test). **F,** *Ex vivo* NIR-PIT in MC38 tumors. The percentage of each lymphocyte subtype among PD-1$^+$ T cells was determined by flow cytometry ($n = 5$ per group; *, $P < 0.05$; ****, $P < 0.0001$; ns, not significant; unpaired t test). Each dot represents an individual sample (tumor), means ± SEM are also shown.

cell segmentation and phenotyping features were used to identify cell phenotypes based on the following criteria: Cancer cells (CK^+CD45^-), $CD8^+$ T cells ($CD8^+$), Tconv ($CD4^+FoxP3^-$), and Treg ($CD4^+FoxP3^+$). For each specimen, at least five pictures were taken, and tissue area and cell count were totaled for each tissue type. The cell density was determined by counting the number of cells per square millimeter.

Statistical analysis

Data are expressed as means ± SEM unless otherwise indicated. Statistical analysis was performed with GraphPad Prism (ver. 8.4.3, GraphPad Software). For multiple-group comparison with one-time measurement, a one-way ANOVA followed by Dunnett's test or Tukey's test was used. For comparison of tumor volumes, repeated measures two-way ANOVA followed by Sidak's test (two groups) or Tukey's test (three or more groups) was used. To analyze immune correlative effects of CD8β-targeted NIR-PIT with anti–PD-1 for a bilateral model, a paired *t* test was used. *P* values less than 0.05 were considered significant.

Data availability

The data generated in this study are available within the article and its Supplementary Data Files or from the corresponding author upon reasonable request.

Results

APC synthesis and antigen-specific localization of anti–CD8β-IR700 in T cells

IR700 conjugation to anti-CD8β to generate anti–CD8β-IR700 was confirmed by SDS-PAGE, which showed IR700 fluorescence only in anti–CD8β-IR700 samples (**Fig. 1A**). Anti–CD8β-IR700 and nonconjugated anti-CD8β had approximately the same molecular weight (**Fig. 1A**). Next, we tested the binding specificity of anti–CD8β-IR700 on T cells collected from lymph nodes. A bright IR700 fluorescence signal was detected in the $CD3\varepsilon^+CD8\alpha^+$ cell population by flow cytometry analysis. This fluorescence signal was completely blocked by the addition of excess nonconjugated anti-CD8β, indicating that the binding of anti–CD8β-IR700 was specific (**Fig. 1B**).

Ex vivo effect of CD8β-targeted NIR-PIT for T cells

To detect the antigen-specific localization and effect of CD8β-targeted NIR-PIT, lymph node T cells were incubated with KIRAVIA Blue 520-conjugated anti-CD4 and anti–CD8β-IR700. Fluorescence microscopy showed that anti–CD8β-IR700 bound to CD4-negative T cells (**Fig. 1C**). After NIR light irradiation, the anti–CD8β-IR700 bound T cells showed swelling, whereas no morphological changes were observed in T cells not bound by anti–CD8β-IR700 (**Fig. 1C**).

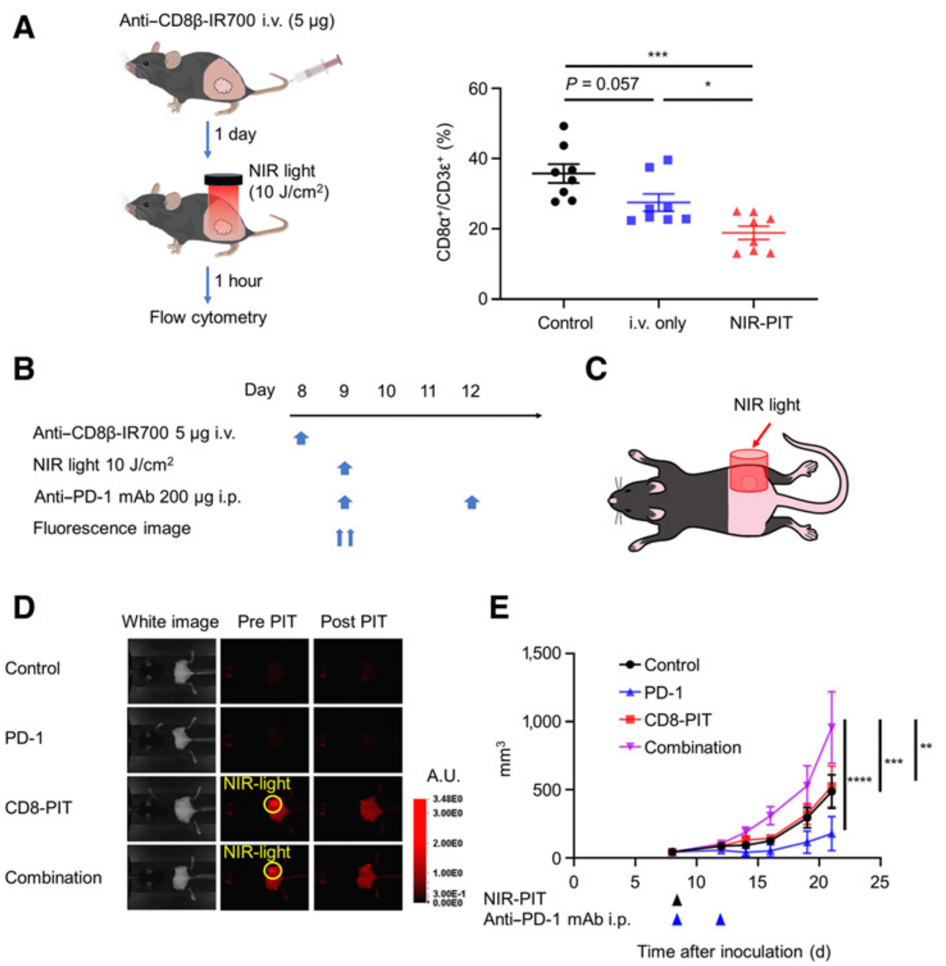

Figure 2.
CD8β-targeted NIR-PIT combined with anti–PD-1 caused tumor progression in MC38 tumors. **A,** Anti–CD8β-IR700 was administered through the tail vein (i.v. injection), and NIR light irradiation was performed the following day. $CD8\alpha^+/CD3\varepsilon^+$ ratios of tumor-infiltrating T cells were analyzed one hour after the NIR light irradiation via flow cytometry (n = 6–7 per group; *, $P < 0.05$; one-way ANOVA followed by the Tukey's test). **B** and **C,** Scheme of CD8β-targeted NIR-PIT combined with anti–PD-1. **D,** *In vivo* IR700 fluorescence imaging of tumor-bearing mice before and after NIR-PIT. The yellow circles indicate the irradiated areas. **E,** Tumor growth curves (n = 10 per group; ****, $P < 0.0001$; ***, $P < 0.001$; **, $P < 0.01$; two-way ANOVA followed by the Tukey's test). Each value represents means ± SEM of independent samples.

Also, PI staining became positive in anti–CD8β-IR700 bound T cells after NIR light irradiation, showing that cell membrane integrity was lost in these cells (**Fig. 1C**).

We also tested the effect of various NIR light doses on the ability of CD8β-targeted NIR-PIT to modulate CD8$^+$ T-cell depletion. Flow cytometry showed that the proportion of CD8α$^+$ cells among CD3ε$^+$ live cells was significantly lower with APC and NIR light (**Fig. 1D**). Without anti–CD8β-IR700, there was no significant difference in the CD8α$^+$/CD3ε$^+$ ratio between 0 J/cm^2 and 30 J/cm^2 (**Fig. 1D**). These results confirmed that no cytotoxicity was induced by NIR light exposure alone, which is consistent with previous work that used other APCs (6, 13, 16). We also examined the effect of CD8β-targeted NIR-PIT on PD-1$^+$ T-cell populations in tumors. Nearly 90% of CD4$^+$FoxP3$^+$ cells (Tregs) in MC38 tumors expressed PD-1, whereas around 60% of CD8α$^+$ T cells and CD4$^+$FoxP3$^-$ conventional T cells (Tconv) expressed PD-1 (**Fig. 1E**; Supplementary Fig. S1). *Ex vivo*

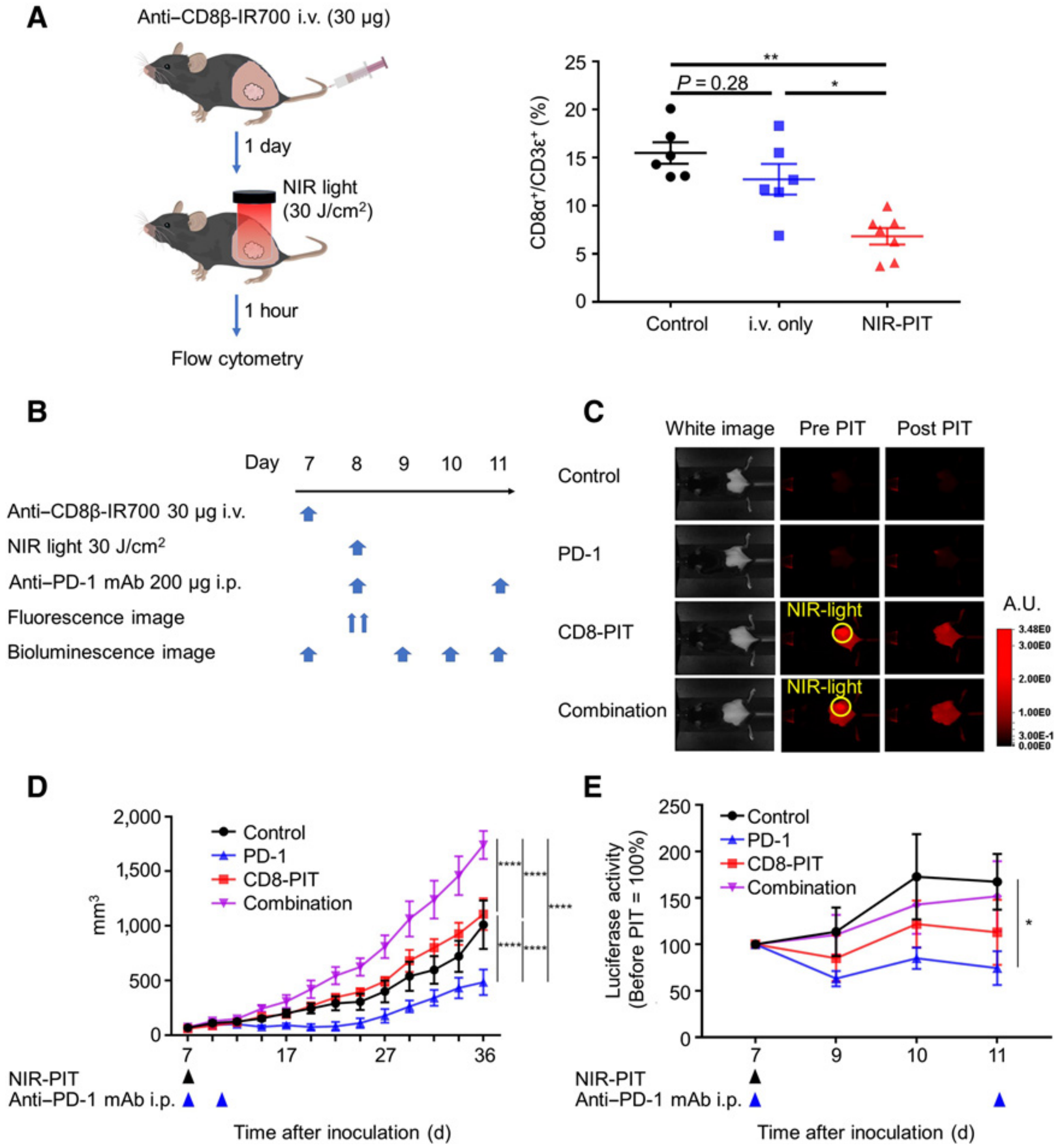

Figure 3.

CD8β-targeted NIR-PIT combined with anti–PD-1 caused tumor progression in MOC2-luc tumors. **A,** Anti–CD8β-IR700 was administered through the tail vein, and NIR light irradiation was performed the following day. CD8α$^+$/CD3ε$^+$ ratios of tumor-infiltrating T cells were determined via flow cytometry ($n = 6$–7 per group; **, $P < 0.01$, *, $P < 0.05$; one-way ANOVA followed by the Tukey's test). **B,** CD8β-targeted NIR-PIT combined with anti–PD-1 regimen. BLI images were obtained at each time point as indicated. **C,** *In vivo* IR700 fluorescence imaging of tumor-bearing mice before and after the NIR-PIT. The yellow circles indicate the NIR light-irradiated areas. **D,** Tumor growth curves ($n = 5$ per group; ****, $P < 0.0001$; two-way ANOVA followed by the Tukey's test). Each value represents means ± SEM of independent samples. **E,** Quantification of luciferase activity in four groups ($n = 5$ per group; *, $P < 0.05$; two-way ANOVA followed by the Tukey's test).

CD8β-targeted NIR-PIT with MC38 tumors showed a significant decrease of PD-1–expressing CD8α$^+$ cells among CD3ε$^+$PD-1$^+$ live cells, no significant change in Tconv, and a significant increase of PD-1–expressing Treg (**Fig. 1F**; Supplementary Fig. S2). This result indicates that after CD8β-targeted NIR-PIT, Tregs are dominant among PD-1$^+$ T cells in the TME.

CD8β-targeted NIR-PIT decreases CD8$^+$ T cells in the TME

We tested the effects of CD8β-targeted NIR-PIT *in vivo*. First, we tested the effect of anti–CD8β-IR700 i.v. injection alone. In lymph node and spleen, the CD8α$^+$/CD3ε$^+$ ratio of the i.v. only group and the NIR-PIT group was lower than that of the control group (Supplementary Fig. S3). To test whether the reduction of the CD8α$^+$/CD3ε$^+$ ratio was a systemic effect of anti–CD8β-IR700, blood samples were taken before and after the anti–CD8β-IR700 injection. A significant decrease in the CD8α$^+$/CD3ε$^+$ ratio was observed one day after 5 μg anti–CD8β-IR700 administration, followed by a gradual recovery over several weeks, suggesting that anti–CD8β-IR700 itself affects the CD8$^+$ T-cell population systemically (Supplementary Fig. S4). Next, we tested the effect of CD8β-targeted NIR-PIT in the TME. In the MC38 tumor model, flow cytometry showed that among tumor-infiltrating lymphocytes (TIL), the CD8α$^+$/CD3ε$^+$ ratio in the NIR-PIT group was lower than that in the control group and the i.v.-only group, whereas no significant difference was seen between the i.v.-only groups and controls (**Fig. 2A**). This suggested that the effect of APC itself in the TME was limited and that NIR-PIT was necessary to deplete CD8$^+$ T cells and cause an imbalance in T-cell subsets within TIL. In contrast, CD8β-targeted NIR-PIT caused no significant decrease in the CD8α-expressing DC population (Supplementary Fig. S5).

Hyperprogression of tumors after the CD8β-targeted NIR-PIT combined with anti–PD-1

We investigated whether combining CD8β-targeted NIR-PIT and anti–PD-1 therapy resulted in rapid tumor growth *in vivo* using subcutaneously implanted MC38, MC38-luc and MOC2-luc tumor models. The treatment regimens and imaging schedules for MC38 and MOC2-luc tumor models are shown in **Fig. 2B**; Supplementary Fig. S6A, respectively. **Figure 2C** is a schematic diagram of the irradiation site. After NIR light irradiation, the fluorescence in the MC38 tumor area decreased to the same level as background with CD8β-targeted NIR-PIT and combination groups (**Fig. 2D**). This means that a sufficient amount of NIR light was delivered to cause photobleaching of the IR700. The posttreatment tumor volumes of the combination group was significantly larger than those of the other 3 groups in the MC38 tumor model (**Fig. 2E**). On the other hand, when MC38-luc tumors were treated with APC 30 μg and NIR laser 30 J/cm^2, excessive tumor growth was observed with CD8β-targeted NIR-PIT

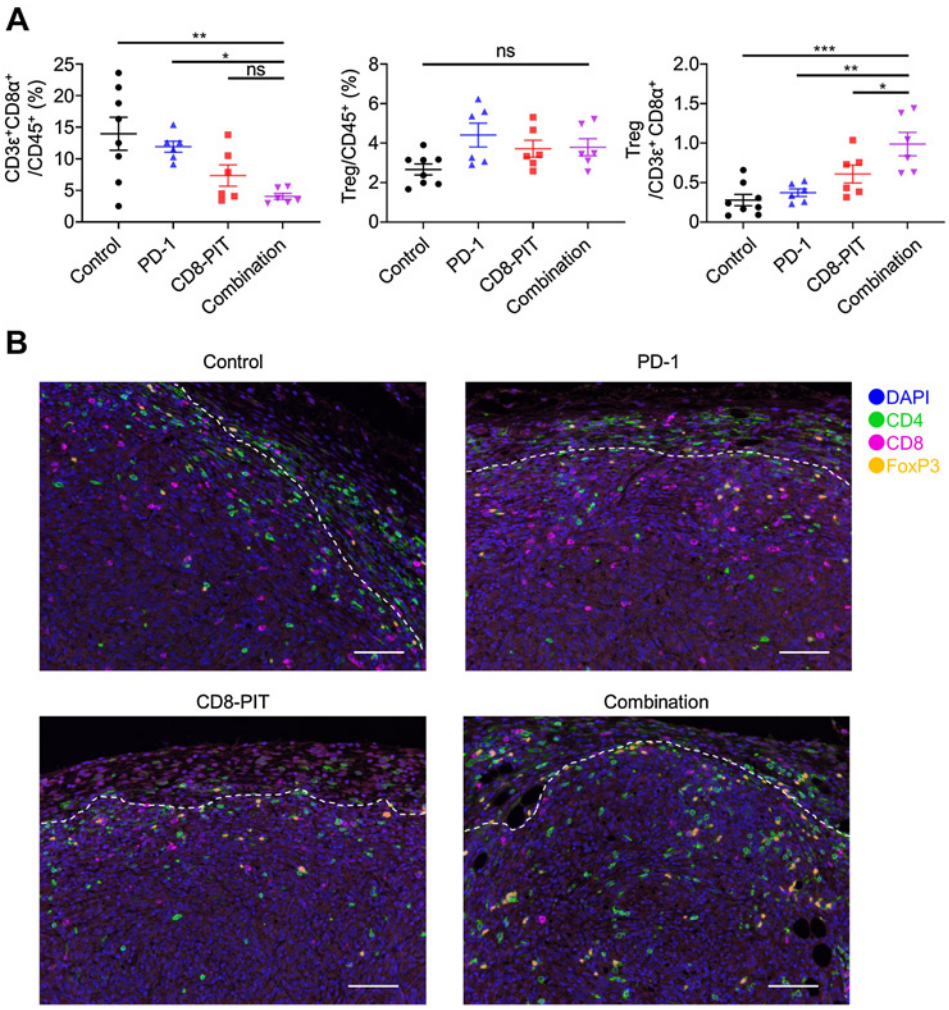

Figure 4.
Effects of CD8β-targeted NIR-PIT and anti–PD-1 on T cells in mice. **A,** MC38 tumors treated with CD8β-targeted NIR-PIT with and without anti–PD-1 and controls were harvested on day 13 (4 days after the NIR light irradiation). CD3ε$^+$CD8α$^+$/CD45$^+$, Treg/CD45$^+$ and Treg/CD3ε$^+$CD8α$^+$ ratios were determined via flow cytometry (n = 6–8 per group; ***, $P < 0.001$; **, $P < 0.01$; *, $P < 0.05$; ns, not significant; vs. combination; one-way ANOVA followed by the Dunnett's test). Each value represents means ± SEM of independent experiments. **B,** MOC2-luc tumors treated with CD8β-targeted NIR-PIT with and without anti–PD-1 and controls were harvested on day 13 (5 days after the NIR light irradiation). Five or more pictures were taken for each tumor and representative composite images of CD8, CD4, FoxP3, and DAPI staining are shown. White dashed line represents tumor border (×200; scale bar, 100 μm).

alone, with no additional effect of anti–PD-1 treatment (Supplementary Fig. S6). MOC2-luc tumor model showed identical results to MC38 tumor models (**Fig. 3**). In addition, the BLI signal indicated that tumor cell activity was lowest in the anti–PD-1 monotherapy group compared with that of the control at day 11 (**Fig. 3E**) in the MOC2-luc tumor model. In the MC38 tumor model, treatment with mild condition (APC 5 μg, NIR light 10 J/cm^2) did not cause excessive tumor growth by itself, on the other hand, in the MC38-luc tumor model, treatment with harsher condition (APC 30 μg and NIR light 30 J/cm^2) promoted tumor growth by CD8β-targeted NIR-PIT itself, with no additional changes seen with anti–PD-1 treatment.

Tumor infiltration of CD8$^+$ T cells and Tregs after combined CD8β-targeted NIR-PIT and anti–PD-1

We tested how TILs were affected after CD8β-targeted NIR-PIT. Flow cytometry analysis in MC38 tumors at day 13 showed that the CD8α$^+$CD3ε$^+$/CD45$^+$ ratio of the combination group was lower than that of the control group and the PD-1 group, suggesting that CD8$^+$ TILs remained low for at least 4 days after CD8β-targeted NIR-PIT (**Fig. 4A**; Supplementary Fig. S7). We also found no significant difference in Treg/CD45$^+$ ratios among the four groups, suggesting that the number of Tregs was not affected by CD8β-targeted NIR-PIT (**Fig. 4A**; Supplementary Fig. S7). As a result, Treg/CD8α$^+$CD3ε$^+$ ratios in the combination group were higher than that of the other 3 groups (**Fig. 4A**). Similar to the flow cytometry data in the MC38 tumors, multiplex IHC of the MOC2-luc tumor model revealed a Treg-dominant intra-tumoral distribution in the combination group (**Fig. 4B**; Supplementary Fig. S8). We also assessed Ki67 expression in CD4$^+$ Tconvs and Tregs to see whether the loss of CD8$^+$ T cells affected the proliferation of other immune cells. We did not see significant change in Ki67 positivity in either of the CD4$^+$ cell populations (Supplementary Fig. S9).

DC activation/maturation after combined CD8β-targeted NIR-PIT and anti–PD-1

We tested how DC activation/maturation status was affected by CD8β-targeted NIR-PIT. Flow cytometry analysis of MC38 tumors on day 13 showed increased CD80 expression in the PD-1 group, whereas CD40 and CD86 expressions were significantly decreased in the CD8-PIT and combination groups (**Fig. 5A**; Supplementary Fig. S10). In addition, analysis of DCs in the tumor-draining lymph nodes showed increased expression of CD40 in the PD-1 group, whereas CD86

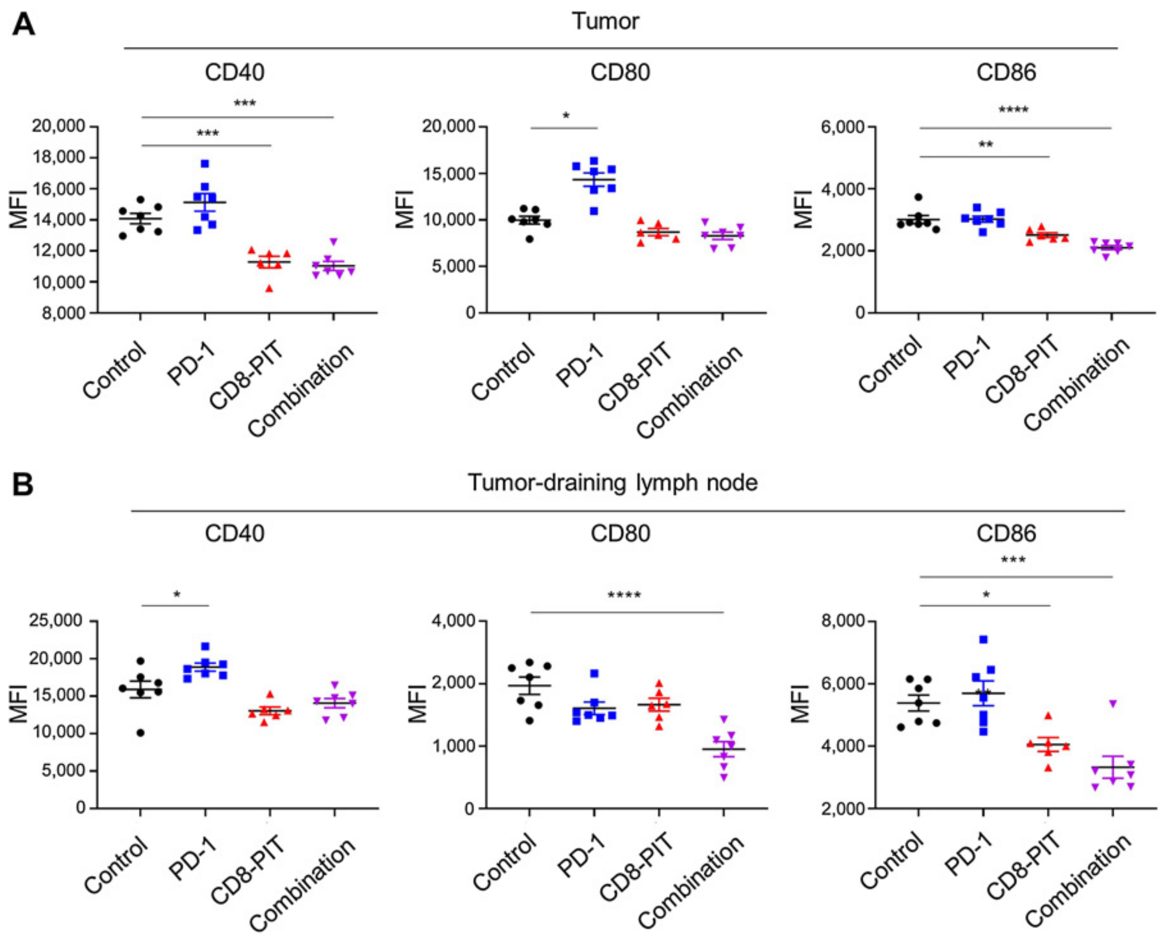

Figure 5.

Effects of CD8β-targeted NIR-PIT and anti–PD-1 on DC activation/maturation. MC38 tumors treated with CD8β-targeted NIR-PIT with and without anti–PD-1 and controls were harvested on day 13 (4 days after the NIR light irradiation). At the same time, tumor-draining lymph nodes were harvested. CD40, CD80, and CD86 expression on DC were analyzed via flow cytometry in intratumoral tissues (**A**) and tumor-draining lymph nodes (**B**). ($n = 6$–7 per group; ****, $P < 0.0001$; ***, $P < 0.001$; **, $P < 0.01$; *, $P < 0.05$; one-way ANOVA followed by Tukey's test). Each value represents means ± SEM of independent experiments.

expression was significantly decreased in the CD8-PIT and combination groups, and CD80 expression was significantly decreased only in the combination group (**Fig. 5B**; Supplementary Fig. S10). These data suggest CD8β-targeted NIR-PIT resulted in impaired DC activation/maturation in tumors and tumor-draining lymph nodes, and that the addition of anti–PD-1 further suppressed activation/maturation of DCs. This result suggests that adding anti–PD-1 to CD8β-based NIR-PIT causes impaired immune activation via suppression of DCs.

CD8β-targeted NIR-PIT combined with anti–PD-1 in a bilateral tumor model

We tested whether the hyperprogression of tumors observed after the combination of CD8β-targeted NIR-PIT and anti–PD-1 therapy was locally restricted or could affect other tumors in the same animal that were not treated with NIR-PIT. **Figure 6A** shows the regimen, imaging schedule, and schematic diagram. Only the tumors on the right flank were irradiated with NIR light; anti–PD-1 was administered intraperitoneally. The fluorescence of the irradiated tumor on the right side was attenuated to the same level as the background, whereas no fluorescence attenuation was observed in the tumor on the left flank, which had been covered with aluminum foil during NIR light exposure (**Fig. 6B**). The posttreatment tumor volume of the NIR-light irradiated side was significantly larger than that of the unirradiated side (**Fig. 6C**). Flow cytometry analysis at day 13 (4 days after NIR-PIT) showed that the CD3ε$^+$CD8α$^+$/CD45$^+$ ratio of the NIR-light irradiated right flank tumors was lower than that of the unirradiated left flank tumors. No significant difference in Treg/CD45$^+$ ratios was observed; however, the Ki67 high/Treg ratio was significantly higher in the NIR-light irradiated tumors (**Fig. 6D**; Supplementary Fig. S11). This result suggests that CD8β-targeted NIR-PIT caused a local imbalance between CD8$^+$ T cells and Tregs in the TME mainly by depleting CD8$^+$ T cells.

Discussion

In this study, we show that CD8β-targeted NIR-PIT specifically depleted intratumoral CD8$^+$ T cells. Moreover, a combination regimen of both CD8β-targeted NIR-PIT and PD-1 blockade

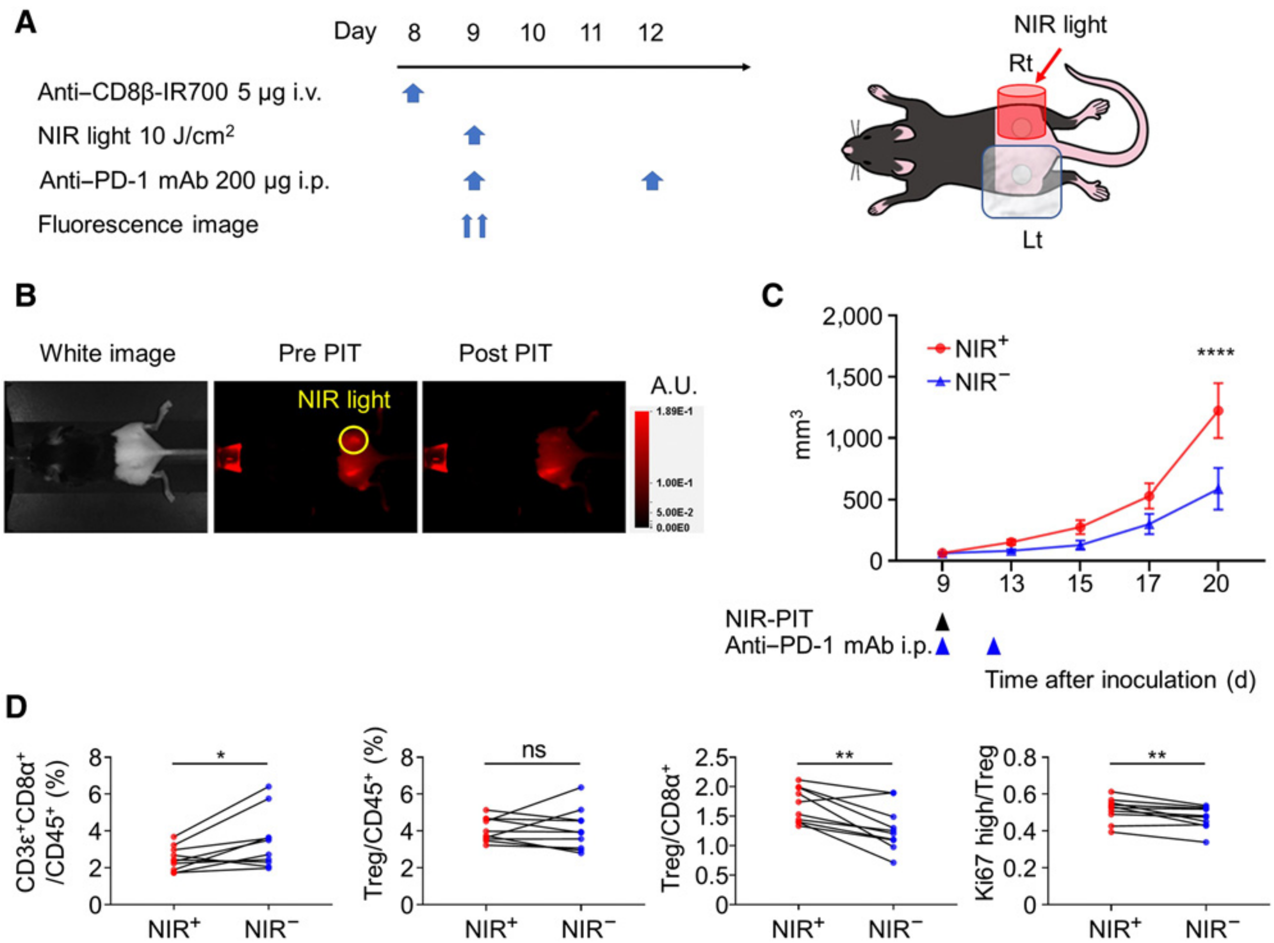

Figure 6.

CD8β-targeted NIR-PIT combined with anti–PD-1 in a bilateral tumor model. **A,** CD8β-targeted NIR-PIT combined with anti–PD-1. MC38 tumors were established in both flanks, NIR-light was administered to the right-flank tumor only. Left-flank tumors were shielded with aluminum foil. **B,** *In vivo* IR700 fluorescence imaging of tumor-bearing mice before and after the NIR-PIT. These pictures are representative of the 10 tumors in each group. The yellow circle indicates the NIR light-irradiated area. **C,** Tumor growth curves ($n = 10$ per group; ****, $P < 0.0001$; two-way ANOVA followed by the Sidak test). Each value represents means ± SEM of independent experiments. **D,** The NIR$^+$ tumors and NIR$^-$ tumors were harvested on day 13. CD3ε$^+$CD8α$^+$/CD45$^+$, Treg/CD45$^+$, Treg/CD3ε$^+$CD8α$^+$, and Ki67high/Treg ratios were analyzed via flow cytometry. ($n = 10$ per group; **, $P < 0.01$; *, $P < 0.05$; ns, not significant; paired t test).

resulted in increased tumor growth compared with PD-1 blockade alone or CD8β-targeted NIR-PIT alone, thus simulating HPD. On day 13, the Treg/CD3ε$^+$CD8α$^+$ ratio of the combination group was higher than that in the other groups because of depletion of CD8$^+$ T cells. Because there was no significant change in Ki67 positivity in CD4$^+$ Tconvs and Tregs after CD8β-targeted NIR-PIT in unilateral MC38 tumor model, the increase in the Treg/CD3ε$^+$CD8α$^+$ ratio was likely to be a result of the reduced number of CD8$^+$ T cells, not because of increased proliferation of nondepleted lymphocytes. We also showed that DC activation/maturation was lower in the CD8β-targeted NIR-PIT and combination groups, suggesting that anticancer immune activation was impaired. Furthermore, in a bilateral tumor model, CD8β-targeted NIR-PIT combined with PD-1 blockade showed more rapid tumor growth on the irradiated side but not the non-irradiated side. Thus, CD8β-targeted NIR-PIT can locally dysregulate the normal balance between effector CD8$^+$ T cells and Tregs creating a Treg-dominant condition in the TME, resulting in rapid tumor progression resembling HPD and thus, this is a potential animal model for HPD.

NIR-PIT has been shown to be effective with a variety of different antibodies targeting numerous tumor antigens (10, 17). A first-in-human phase 1/2 clinical trial of NIR-PIT using cetuximab-IR700 (RM-1929), which targets epidermal growth factor receptor (EGFR), in patients with inoperable head and neck squamous cell cancer concluded in late 2017 (NCT02422979). Early results suggest that NIR-PIT is superior to existing second- and third-line therapies for recurrent head and neck cancers (18). A global phase 3 clinical trial of NIR-PIT using cetuximab-IR700 (ASP-1929), which targets EGFR, began in 2018 in patients with recurrent head and neck cancer who have failed at least first-line therapy (NCT03769506). In September 2020, the first APC for clinical use, a cetuximab-IR700 conjugate referred to as Akalux (Rakuten Medical Inc.), and a NIR laser system (BioBlade, Rakuten Medical Inc.) were approved for clinical use by the Pharmaceuticals and Medical Devices Agency in Japan. Thus, NIR-PIT appears to be a promising new cancer therapy.

NIR-PIT can also be directed against host immune cell subpopulations in the TME (19–22). NIR-PIT, therefore, could become a new tool for studying experimental immunobiology. No other method can quickly and selectively eliminate a single type of cell within the TME within 20 minutes, thereby dramatically altering the local balance of cell populations. Such rapid depletion of a single type of cell could be useful in investigating the functions of specific cell types in the TME. In this study, we used NIR-PIT to selectively deplete CD8$^+$ T cells to alter the balance between CD8$^+$ T cells and Tregs. This method can be adjusted to create delicate balance in TME. The NIR-PIT in harsher condition (e.g., more NIR light) can deplete more CD8$^+$ T cells, as shown in *ex vivo* CD8β-targeted NIR-PIT. In this study, the suitable condition of CD8$^+$ T-cell depletion to simulate HPD was different in different tumor models, for example, the treatment condition that successfully simulate HPD with anti–PD-1 treatment in MOC2-luc model induced similar tumor overgrowth by CD8$^+$ T-cell depletion alone. This suggests that there is a tumor-specific sweet spot in the ratio of CD8$^+$ T cells to Tregs in tumors where anti–PD-1 induces tumor growth. Such sweet spots might be determined by characteristics such as the starting amount of CD8$^+$ T cells or tumor growth speed. Our previous study showed MC38-luc contained more CD8$^+$ T cells than MOC2-luc, this study showed that the growth of MC38-luc was faster than for the other two models. With the balance thus altered, we showed that subsequent PD-1 blockade could accelerate tumor growth providing a model of HPD that can be seen clinically with PD-1 blockade therapy.

Previous studies based on IHC have documented an association between CD8$^+$ T cells in tumors and response to ICIs in melanoma and colorectal cancer (23, 24). Our results similarly showed that reducing the proportion of CD8$^+$ T cells in the TME with CD8β-targeted NIR-PIT caused a reversal of the therapeutic effect of anti–PD-1. Moreover, the combination of CD8β-targeted NIR-PIT and anti–PD-1 therapy resulted in rapid tumor growth. Kamada and colleagues (5) showed that Ki67 expression by PD-1$^+$ effector Tregs was increased after PD-1 blockade. The study also suggested that PD-1 blockade facilitated the proliferation of highly suppressive PD-1$^+$ effector Tregs in the setting of HPD, resulting in inhibition of antitumor immunity (5). Similarly, in our study, Ki67 positivity in Tregs tended to be higher with anti–PD-1 treatment, although the difference was not statistically significant. Considering the previous study, we hypothesize that the proliferation status of PD-1$^+$ effector Treg could be enhanced by PD-1 blockade,

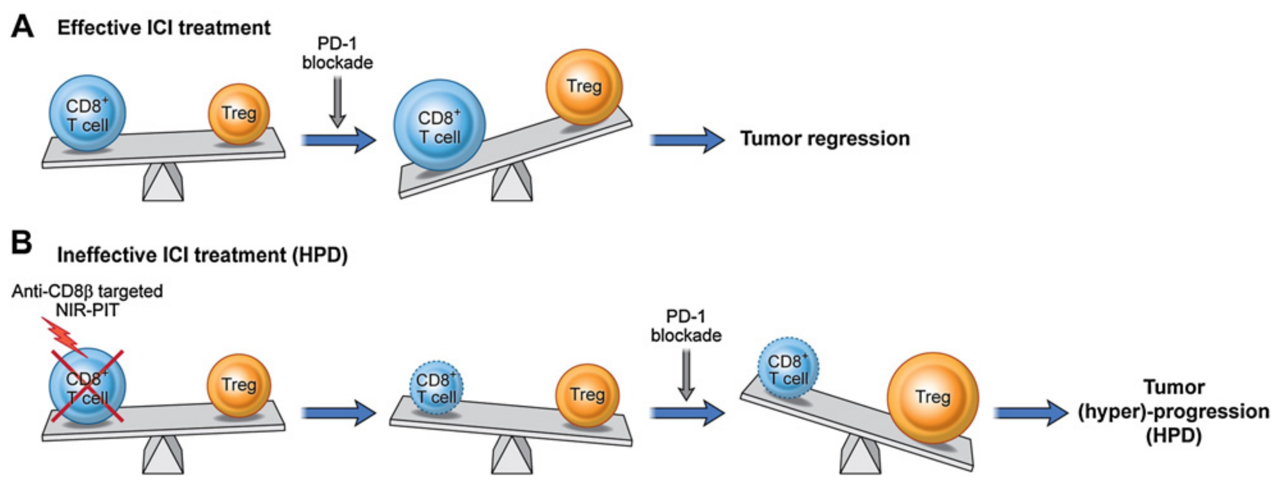

Figure 7.

A proposed model showing how CD8β-targeted NIR-PIT combined with anti–PD-1 could induce tumor progression. The imbalance between CD8$^+$ T cells and Tregs could be a reason for HPD after PD-1 blockade therapy.

which could explain why tumor progression in the combination group was more rapid than in the CD8β-targeted NIR-PIT monotherapy group (**Fig. 7**).

In this study, we used CD8β-specific mAbs for anti–CD8β-IR700. The $CD8\alpha^+/CD3\varepsilon^+$ ratio in the tumor was not affected by anti–CD8β-IR700 injection without NIR-light exposure; however, the $CD8\alpha^+/CD3\varepsilon^+$ ratio in the lymph node, spleen, and peripheral blood was significantly reduced. We think the decreased $CD8\alpha^+/CD3\varepsilon^+$ ratio in the lymph node, spleen, and peripheral blood was caused by Fc-mediated antibody-dependent cellular cytotoxicity (ADCC) or complement-dependent cytotoxicity (25). The reasons ADCC-mediated cell depletion were less apparent in tumors is likely because: (i) ADCC-mediating cells may be dysfunctional in the TME (26, 27); (ii) ADCC-mediating cells such as NK cells and macrophages are more abundant in lymphatic tissues. When we test the effect of local depletion of $CD8^+$ T cells, it would be ideal if the effect of CD8β-targeted NIR-PIT was completely local without systemic cell depletion. To achieve such a local depletion, we could use IR700-conjugated anti–CD8β-F(ab′)$_2$, which does not have an Fc region (16). However, IR700-conjugated anti–CD8β-F(ab′)$_2$ could be less effective because of more rapid clearance from the circulation. Thus, further studies are needed to confirm whether NIR-PIT using IR700-conjugated anti-CD8β-F(ab′)$_2$ could reduce the number of tumor-infiltrating $CD8^+$ T cells and cause HPD with PD-1 blockade.

The findings in this study lead to some hypotheses concerning HPD in human patients. For example, it could be that in some patients, the pre-existing relative balance of $CD8^+$ T cells and Tregs may be such that the addition of PD-1 blockade changes the relative balance within the TME leading to a Treg-dominant environment. This would be highly permissive of tumor growth and could result in HPD. Alternatively, in some patients, the addition of PD-1 blockade could stimulate Treg proliferation, thus also resulting in HPD. It would be highly desirable to understand the critical point of equipoise between $CD8^+$ effector T cell–dominant and Treg-dominant TMEs to better predict HPD. For actual application to patients, reviewing the Treg/$CD8^+$ T-cell ratio in pretreatment biopsies might allow clinicians to predict the probability of HPD. In cases that high Treg/$CD8^+$ T cell ratios are observed, reducing the number of Tregs by Treg-targeted NIR-PIT (e.g., CD25-targeted NIR-PIT) before anti–PD-1 administration may reduce the likelihood of HPD. Moreover, it is possible that the Treg/$CD8^+$ T-cell balance could be tipped either way by any potentially immunosuppressive treatment, thus, this experiment may mimic a treatment that result in a higher Treg/$CD8^+$ T-cell ratio. We should be aware of HPD during such treatments.

In conclusion, we generated an animal model with a Treg-dominant TME by partially eliminating $CD8^+$ T cells using CD8β-targeted NIR-PIT, which led to rapid tumor growth resembling HPD when combined with anti–PD-1 therapy. This result suggests that an imbalance of Treg/$CD8^+$ T cells may be responsible for HPD, which is an occasional but highly unfortunate outcome of PD-1 blockade therapy. We believe the model described here will be useful for the future study of HPD.

Authors' Disclosures

No disclosures were reported.

Authors' Contributions

H. Wakiyama: Data curation, formal analysis, validation, investigation, writing–original draft. **T. Kato:** Investigation, methodology. **A. Furusawa:** Data curation, investigation, methodology, writing–original draft, writing–review and editing. **R. Okada:** Data curation, investigation. **F. Inagaki:** Investigation, methodology. **H. Furumoto:** Investigation. **H. Fukushima:** Investigation. **S. Okuyama:** Investigation. **P.L. Choyke:** Validation, project administration, writing–review and editing. **H. Kobayashi:** Conceptualization, resources, data curation, formal analysis, supervision, funding acquisition, validation, investigation, methodology, writing–original draft, project administration, writing–review and editing.

Acknowledgments

This research was supported by the Intramural Research Program of the National Institutes of Health, National Cancer Institute, Center for Cancer Research (ZIA BC 011513). F. Inagaki was also supported with a grant from National Center for Global Health and Medicine Research Institute, Tokyo, Japan.

The publication costs of this article were defrayed in part by the payment of publication fees. Therefore, and solely to indicate this fact, this article is hereby marked "advertisement" in accordance with 18 USC section 1734.

Note

Supplementary data for this article are available at Cancer Immunology Research Online (http://cancerimmunolres.aacrjournals.org/).

Received January 13, 2022; revised June 13, 2022; accepted September 8, 2022; published first October 11, 2022.

References

1. Champiat S, Dercle L, Ammari S, Massard C,Hollebecque A, Postel-Vinay S, et al. Hyperprogressive disease is a new pattern of progression in cancer patients treated by anti–PD-1/PD-L1. Clin Cancer Res 2017;23:1920–8.
2. Matos I, Martin-Liberal J, Hierro C, Olza MOD, Viaplana C, Costa M, et al. Incidence and clinical implications of a new definition of hyperprogression (HPD) with immune checkpoint inhibitors (ICIs) in patients treated in phase 1 (Ph1) trials. J Clin Oncol 2018;36:3032.
3. Adashek JJ, Subbiah IM, Matos I, Garralda E, Menta AK, Ganeshan DM, et al. Hyperprogression and immunotherapy: fact, fiction, or alternative fact? Trends Cancer 2020;6:181–91.
4. Kas B, Talbot H, Ferrara R, Richard C, Lamarque JP, Pitre-Champagnat S, et al. Clarification of definitions of hyperprogressive disease during immunotherapy for non–small cell lung cancer. JAMA Oncol 2020;6:1039–46.
5. Kamada T, Togashi Y, Tay C, Ha D, Sasaki A, Nakamura Y, et al. PD-1(+) regulatory T cells amplified by PD-1 blockade promote hyperprogression of cancer. Proc Natl Acad Sci U S A 2019;116:9999–10008.
6. Mitsunaga M, Ogawa M, Kosaka N, Rosenblum LT, Choyke PL, Kobayashi H. Cancer cell-selective *in vivo* near infrared photoimmunotherapy targeting specific membrane molecules. Nat Med 2011;17:1685–91.
7. Kobayashi H, Choyke PL. Near-Infrared Photoimmunotherapy of Cancer. Acc Chem Res 2019;52:2332–9.
8. Ogawa M, Tomita Y, Nakamura Y, Lee MJ, Lee S, Tomita S, et al. Immunogenic cancer cell death selectively induced by near infrared photoimmunotherapy initiates host tumor immunity. Oncotarget 2017;8:10425–36.
9. Mitsunaga M, Nakajima T, Sano K, Kramer-Marek G, Choyke PL, Kobayashi H. Immediate *in vivo* target-specific cancer cell death after near infrared photoimmunotherapy. BMC Cancer 2012;12:345.
10. Kato T, Wakiyama H, Furusawa A, Choyke PL, Kobayashi H. Near-infrared photoimmunotherapy; a review of targets for cancer therapy. Cancers 2021,13.
11. Vremec D, Zorbas M, Scollay R, Saunders DJ, Ardavin CF, Wu L, et al. The surface phenotype of dendritic cells purified from mouse thymus and spleen: investigation of the CD8 expression by a subpopulation of dendritic cells. J Exp Med 1992;176:47–58.

12. Maruoka Y, Furusawa A, Okada R, Inagaki F, Fujimura D, Wakiyama H, et al. Combined CD44- and CD25-targeted Near-infrared photoimmunotherapy selectively kills cancer and regulatory T cells in syngeneic mouse cancer models. Cancer Immunol Res 2020;8:345–55.
13. Nagaya T, Nakamura Y, Okuyama S, Ogata F, Maruoka Y, Choyke PL, et al. Syngeneic mouse models of oral cancer are effectively targeted by anti–CD44-based NIR-PIT. Mol Cancer Res 2017;15:1667–77.
14. Maruoka Y, Nagaya T, Nakamura Y, Sato K, Ogata F, Okuyama S, et al. Evaluation of early therapeutic effects after near-infrared photoimmunotherapy (NIR-PIT) using luciferase–luciferin photon-counting and fluorescence imaging. Mol Pharm 2017;14:4628–35.
15. Wakiyama H, Furusawa A, Okada R, Inagaki F, Kato T, Maruoka Y, et al. Increased immunogenicity of a minimally immunogenic tumor after cancer-targeting near infrared photoimmunotherapy. Cancers 2020;12:3747.
16. Okada R, Maruoka Y, Furusawa A, Inagaki F, Nagaya T, Fujimura D, et al. The effect of antibody fragments on CD25 targeted regulatory T-cell near-infrared photoimmunotherapy. Bioconjug Chem 2019;30:2624–33.
17. Wakiyama H, Kato T, Furusawa A, Choyke PL, Kobayashi H. Near infrared photoimmunotherapy of cancer; possible clinical applications. Nanophotonics 2021;10:3135–51.
18. Cognetti DM, Johnson JM, Curry JM, Kochuparambil ST, McDonald D, Mott F, et al. Phase 1/2a, open-label, multicenter study of RM-1929 photoimmunotherapy in patients with locoregional, recurrent head and neck squamous cell carcinoma. Head Neck 2021;43:3875–87.
19. Sato K, Sato N, Xu B, Nakamura Y, Nagaya T, Choyke PL, et al. Spatially selective depletion of tumor-associated regulatory T cells with near-infrared photoimmunotherapy. Sci Transl Med 2016;8:352ra110.
20. Okada R, Kato T, Furusawa A, Inagaki F, Wakiyama H, Choyke PL, et al. Local depletion of immune checkpoint ligand CTLA4-expressing cells in tumor beds enhances antitumor host immunity. Adv Ther 2021;4:2000269.
21. Kobayashi H, Furusawa A, Rosenberg A, Choyke PL. Near-infrared photoimmunotherapy of cancer: a new approach that kills cancer cells and enhances anticancer host immunity. Int Immunol 2021;33:7–15.
22. Kato T, Okada R, Furusawa A, Inagaki F, Wakiyama H, Furumoto H, et al. Simultaneously combined cancer cell- and CTLA4-targeted NIR-PIT causes a synergistic treatment effect in syngeneic mouse models. Mol Cancer Ther 2021;20:2262–73.
23. Tumeh PC, Harview CL, Yearley JH, Shintaku IP, Taylor EJ, Robert L, et al. PD-1 blockade induces responses by inhibiting adaptive immune resistance. Nature 2014;515:568–71.
24. Le DT, Uram JN, Wang H, Bartlett BR, Kemberling H, Eyring AD, et al. PD-1 blockade in tumors with mismatch-repair deficiency. N Engl J Med 2015;372:2509–20.
25. Weiner LM, Surana R, Wang S. Monoclonal antibodies: versatile platforms for cancer immunotherapy. Nat Rev Immunol 2010;10:317–27.
26. Melaiu O, Lucarini V, Cifaldi L, Fruci D. Influence of the tumor microenvironment on NK cell function in solid tumors. Front Immunol 2019;10:3038.
27. Sica A, Bronte V. Altered macrophage differentiation and immune dysfunction in tumor development. J Clin Invest 2007;117:1155–66.